Reduced copper transporter trafficking and synaptic deficits in iPSC-MNs derived from an ALS patient with a novel variant of ATP7A

A. STARR[1], N. BAKKAR[1], Z. T. MCEACHIN[2], I. LORENZINI[1], R. REIMAN[3], E. HUTCHENS[3], K. VAN-KEUREN JENSEN[3], G. J. BASSELL[2], N. M. BOULIS[2], R. SATTLER[1], R. BOWSER[1]

[1]Division of Neurobiology, Barrow Neurological Institute, Phoenix, AZ; [2]Emory University, Atlanta, GA; [3]Translational Genomics Research Institute, Phoenix, AZ

Introduction

Dysregulation of copper distribution has been discovered in a number of neurological diseases, including Menke's disease, Alzheimer's disease, and a distal motor neuropathy. Due to its role in mitochondrial function, antioxidant activity, and synaptic transmission, changes in copper homeostasis can cause a broad range of cognitive and motor deficits. Mutations in the P-type ATPase copper transporter ATP7A are known to cause Menke's disease, occipital horn syndrome, and X-linked spinal muscular atrophy type 3. We previously reported a novel variant of ATP7A in a male patient with brachial amyotrophic diplegia, a slow-progressing form of motor neuron disease. The possible contribution of this mutation to the patient's disease pathogenesis is unknown. The nonsynonymous M1311V substitution, located near the ATP binding site of the protein, is associated with mislocalization of ATP7A at basal levels and impaired trafficking in response to increased copper when overexpressed in HeLa cells and in patient fibroblasts. No changes in ATP7A transcript or gene expression were observed in fibroblasts. Patient fibroblasts were reprogrammed into induced pluripotent stem cells and differentiated into motor neurons (iPS-MNs). This model was used to examine ATP7A expression and localization in a more disease-relevant cell type. In addition, we examined morphological and functional parameters commonly affected in ALS and other ATP7A-associated diseases, namely, dendritic morphology, hyperexcitability, and excitotoxicity. Due to copper's previously established role as a local modulator of glutamate receptor expression, distribution, and permeability, changes in transporter trafficking could explain changes in synaptic function. Further work will be required to determine if changes in ATP7A protein expression or trafficking cause a toxic level of copper redistribution capable of contributing to the observed physiological deficits and, ultimately, ALS.

Proposed Role of ATP7A in Motor Neurons

(Kaler, S. G. *Nature Rev. Neurology* 2011)

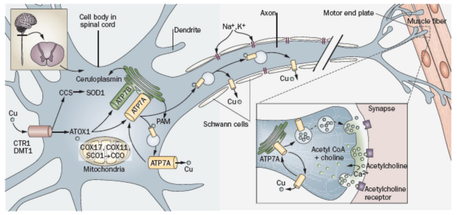

Methods

RNA Sequencing

RNA was isolated using the RNAqueous Phenol-free total RNA Isolation Kit. cDNA synthesis and library prep were performed using a SMARTer and KAPA Hyper kit combination. Demultiplexing and fastq generation were performed using CASAVA v1.8.4, followed by trimming of 7nt from both R1 and R2 using cutadapt v1.10, as recommended in the SMARTer manual. Reads were then aligned to the GRCh37 human genome using STAR v2.5.2b, and raw counts were calculated with featureCounts (subread v1.5.1) using the ensembl75 annotation. Analysis and differential expression testing were performed in R using DESeq2 v1.14.1.

iPS Motor Neuron Cell Culture Model

Control and p.M1311V patient-derived fibroblasts were reprogrammed into iPS cells, which were then differentiated into motor neurons (Donnelly et. al. *Neuron* 2013). Experiments were conducted on or after day 53 of the differentiation protocol, a time point which has previously proven to generate functional motor neurons.

ATP7A Colocalization with TGN46 and Response to Elevated Copper Concentrations

Control and M1311V fibroblasts and iPSMN's were plated on cover slips. Copper (II) chloride was added to the media to reach the given concentration. After 1 hour, the media was removed and cells were fixed and immunostained. Cells were imaged using a Zeiss confocal microscope with a 63X objective.

Imaris image analysis software was used to quantify the colocalization of ATP7A and the trans-golgi network marker TGN46. After setting fluorescense thresholds to remove background, the Pearson's correlation coefficent of the three-dimensional position of above-threshold pixels in the ATP7A andTGN46 channels were calculated.

Dendritic Length, Sholl Analysis, and Spine Density

Control and M1311V iPS-MNs were cultured on astrocytes and transfected with a lentiviral CMV promoter-driven GFP construct. Cells were treated with virus for 24 hours. They were washed and fixed 48 hours after virus removal and immunostained for MAP2. Cells were imaged using a Zeiss confocal microscope with a 63X objective. Imaris filament trace software was used to trace dendritic filaments, and total denritic length data was extracted from these traces. Traces were then uploaded into ImageJ for Sholl analysis. Spine density was calculated by manually counting the number of spines on a traced cell and dividing by total dendritic length. Spine subtypes were defined as follows: filipodium = total extent > 3µm, thin = 1µm < total extent < 3, mushroom = head diameter > 0.35µm, all others are stubby.

Micro Electrode Array Analysis

Control and M1311V iPS-MNs were cultured on astrocytes and plated on 48-well plates designed for the Axion Biosystems Maestro MEA. Spontaneous spikes (changes in electric field potential > 6 SD above background) were recorded for 5 minutes at multiple time points from day 53 to day 78 of the differentiation. Mean firing rate, mean bursts, and mean network bursts were analyzed.

Results

1. Differentially expressed genes and proteins in ATP7A-M1311V iPS-MNs.

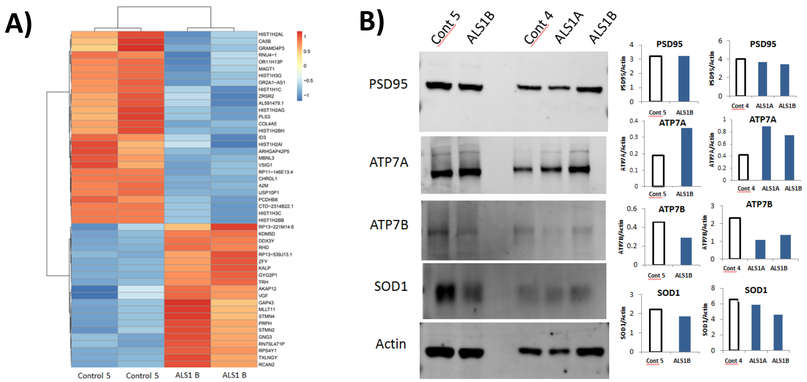

Figure 1. A) Heat map showing differentially expressed genes as determined via duplicate RNA sequencing of M1311V patient-derived (ALS1) and healthy control-derived iPS-MNs. Differentially expressed genes were selected based on the following criteria: adjusted p-values ($p<0.05$), an absolute value of the log2 fold change greater than 1, and a baseMean value greater than 20. Heatmaps were generated using the pheatmap v1.0.8 R package. **B)** Westerns blots of total protein lysates from 2 M1311V patient iPS-MN clones (ALS1 A and B) and 2 healthy control iPS-MN lines with densitometric quantification normalized to actin using ImageQuant.

2. ATP7A-M1311V fibroblasts and iPS-MNs exhibit mislocalization of ATP7A and decreased ATP7A trafficking in response to elevated copper.

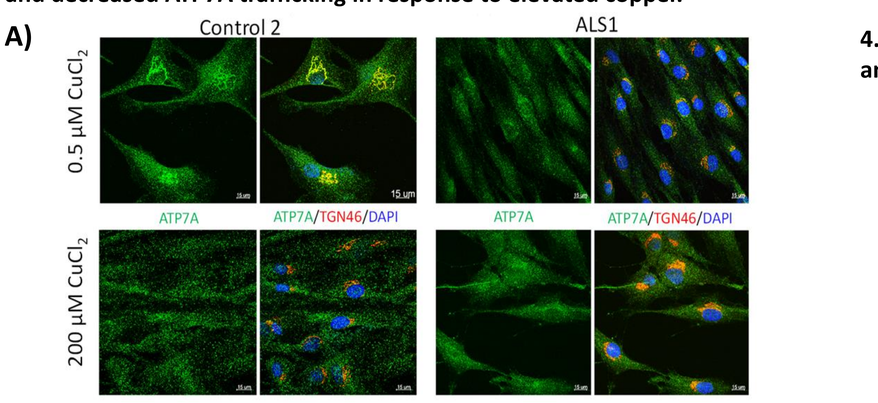

Figure 2. A) Representative confocal microscopy images of healthy control and M1311V patient fibroblasts stained with Anti-ATP7A (Green), Anti-TGN46 (Red), and DAPI (Blue) at 0.5 µM and 200 µM $CuCl_2$ concentration in the media for 1 hour. **B)** Pearson's correlation indicating colocalization of wildtype and M1311V mutant ATP7A protein with the trans-Golgi apparatus marker TGN46. Results indicate a significant reduction of mutant ATP7A protein at the Golgi at basal levels of copper (0.5 µM) and impaired trafficking in response to elevated copper (200µM) (three healthy control and two M1311V fibroblast lines, ALS1 and a line carrying the mutation provided by the NIH, n>30 per line). **C) & D)** Colocalization of ATP7A with TGN46 in M1311V patient-derived iPS-MNs and healthy controls. Results reflect findings in fibroblasts of reduced ATP7A at the Golgi at basal (0.5 µM) copper levels and impaired trafficking in response to elevated copper (200 µM). Results from 2 separate differentiations of 1 M1311V clone and 1 control shown, n>20 cells per line/treatment.

3. ATP7A-M1311V iPS-MNs exhibit morphological deficits.

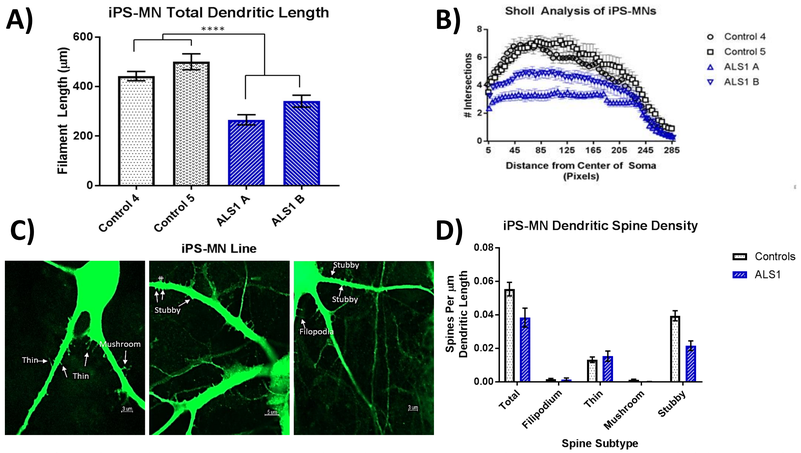

Figure 3. A) Quantification of total dendritic length in traces of 2 healthy controls and 2 clones of M1311V iPS-MNs (n=20 per line). **B)** Sholl analysis of dendritic traces of 2 healthy controls and 2 clones of M1311V iPS-MNs, presented as number of intersections with a circle drawn at a given pixel distance from the center of the soma (n=20 per line). **C)** Representative image of iPS-MNs indicating subtypes assigned to different spine morphologies. **D)** Comparison of the density of spines and specific spine subtypes per micron of dendritic length in iPS-MNs from 2 healthy control lines and 2 M1311V clones (N=20 per line).

4. ATP7A-M1311V patient iPS-MNs show age-sensitive changes in excitability and increased sensitivity to glutamate toxicity.

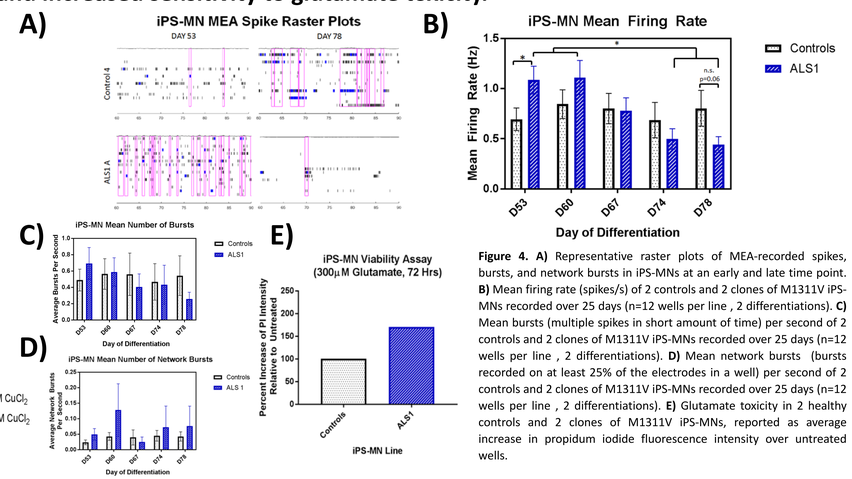

Figure 4. A) Representative raster plots of MEA-recorded spikes, bursts, and network bursts in iPS-MNs at an early and late time point. **B)** Mean firing rate (spikes/s) of 2 controls and 2 clones of M1311V iPS-MNs recorded over 25 days (n=12 wells per line , 2 differentiations). **C)** Mean bursts (multiple spikes in short amount of time) per second of 2 controls and 2 clones of M1311V iPS-MNs recorded over 25 days (n=12 wells per line , 2 differentiations). **D)** Mean network bursts (bursts recorded on at least 25% of the electrodes in a well) per second of 2 controls and 2 clones of M1311V iPS-MNs recorded over 25 days (n=12 wells per line , 2 differentiations). **E)** Glutamate toxicity in 2 healthy controls and 2 clones of M1311V iPS-MNs, reported as average increase in propidum iodide fluorescence intensity over untreated wells.

Conclusions

The M1311V mutation in ATP7A causes mislocalization and impaired trafficking of the protein in response to changes in copper concentration. In addition, M1311V patient iPS-MNs show increased expression of ATP7A and decreased expression of ATP7B. M1311V patient iPS-MNs show deficits in dendritic and spine morphology with accompanying changes in excitability and increased sensitivity to glutamate toxicity. Further work is required to determine if the mislocalization causes changes in copper transport, which has previously been shown to affect synaptic protein expression and distribution and increase excitotoxicity.

Special thanks to S. G. Kaler for providing NIH M1311V fibroblasts & ATP7A cDNA constructs & to N. Twishime and D. Shenoy for quantifying images.

Funding: Above & Beyond, LLC